Title
Critical roles of the immunoglobulin intronic enhancers in maintaining the sequential rearrangement of IgH and Igk loci.

Journal
The Journal of experimental medicine, 203(7)

ISSN
0022-1007

Authors
Inlay, Matthew A
Lin, Tongxiang
Gao, Heather H
et al.

Publication Date
2006-07-01

DOI
10.1084/jem.20052310

Peer reviewed

Critical roles of the immunoglobulin intronic enhancers in maintaining the sequential rearrangement of *IgH* and *Igk* loci

Matthew A. Inlay, Tongxiang Lin, Heather H. Gao, and Yang Xu

Section of Molecular Biology, Division of Biological Sciences, University of California, San Diego, La Jolla, CA 92093

V(D)J recombination of immunoglobulin (Ig) heavy (*IgH*) and light chain genes occurs sequentially in the pro– and pre–B cells. To identify cis-elements that dictate this order of rearrangement, we replaced the endogenous matrix attachment region/*Igk* intronic enhancer (MiE_κ) with its heavy chain counterpart (Eμ) in mice. This replacement, denoted EμR, substantially increases the accessibility of both V_κ and J_κ loci to V(D)J recombinase in pro–B cells and induces *Igk* rearrangement in these cells. However, EμR does not support *Igk* rearrangement in pre–B cells. Similar to that in $MiE_\kappa^{-/-}$ pre–B cells, the accessibility of V_κ segments to V(D)J recombinase is considerably reduced in EμR pre–B cells when compared with wild-type pre–B cells. Therefore, Eμ and MiE_κ play developmental stage-specific roles in maintaining the sequential rearrangement of *IgH* and *Igk* loci by promoting the accessibility of V, D, and J loci to the V(D)J recombinase.

CORRESPONDENCE
Yang Xu:
yangxu@ucsd.edu

Abbreviations used: ChIP, chromatin immunoprecipitation; ES, embryonic stem; GT, germline transcript; hC_κ, human κ constant region; LM, ligation mediated; MAR, matrix attachment region; mC_κ, mouse κ constant region; MiE_κ, MAR/*Igk* intronic enhancer; MSRE-QPCR, methylation-sensitive restriction enzyme real-time quantitative PCR; PGK, phosphoglycerol kinase; RS, recombining sequence; RSS, recombination signal sequence; SE, signal end.

The Ig and TCR genes are assembled through the somatic recombination of V (Variable), D (Diversity), and J (Junction) gene segments during the early stages of lymphocyte development (1). B lymphocytes express one set of the heavy chain (*IgH*) and either the κ or λ light chain loci (*IgL*). V(D)J recombination of the *IgH* and *IgL* chain genes occurs in a sequential manner. *IgH* rearrangement occurs primarily in pro–B cells, and *IgL* rearrangement occurs primarily in pre–B cells (1). The accessibility of each antigen receptor locus to the recombination machinery regulates its timing and efficiency of rearrangement (2–4). During the appropriate developmental stage, chromatin remodeling complexes modify the chromatin structure of the locus and convert it into a state accessible to the V(D)J recombinase (5–7). Such changes in accessibility are thought to be mediated by cis-elements residing within each locus (5).

Both *IgH* and *Igk* loci contain an enhancer between the J segments and the constant region, which are called *IgH* intronic enhancer (Eμ) and matrix attachment region (MAR)/*Igk* intronic enhancer (MiE_κ), respectively (8–12). Both loci also contain multiple other regulatory elements downstream or within their constant region exons. The *Igk* locus contains the $3'E_\kappa$ (13) and Ed (14) enhancers, and the *IgH* locus contains four enhancer elements in its $3'E_H$ regulatory region (hs3a, hs1/2, hs3b, and hs4; references 15–17). The deletion of Eμ in mice severely decreases V_H to DJ_H rearrangement (18–20). The deletion of either MiE_κ or $3'E_\kappa$ from the endogenous *Igk* locus differentially decreases the rearrangement of *Igk* (21, 22). In addition, the deletion of both *Igk* enhancers abolishes *Igk* rearrangement, indicating that these two enhancers play redundant and essential roles in activating *Igk* rearrangement (23).

The mechanisms by which cis-elements activate *Igk* recombination remain unclear. One potential mechanism is through the activation of germline transcription from germline promoters located upstream of J_κ (24–27), as κ^0 germline transcription (κ^0GT [germline transcript]) appears to play a quantitative role in activating *Igk* rearrangement (28, 29). Germline transcription of V_κ gene segments (V_κGT) may also play a role in regulating the accessibility of the V_κ regions (30). Another mechanism could be DNA demethylation (31). In this context, DNA methylation is inversely correlated with the efficiency of *Igk* rearrangement, and *Igk* enhancers are critical for demethylation of the *Igk* locus (23). However, only a minor demethylation of *Igk* can be detected in WT pre–B cells (32), suggesting that demethylation occurs within a small pre–B cell

M.A. Inlay and T. Lin contributed equally to this work.
The online version of this article contains supplemental material.

population immediately before the rearrangement of this locus. Hypomethylation of the *Igk* locus resulting from the targeted deletion of the methyltransferase gene *Dnmt1* is not sufficient to activate *Igk* rearrangement in pre–B cell lines, suggesting that DNA demethylation alone is not sufficient in activating *Igk* rearrangement (33).

Recent studies suggest that histone modification is involved in regulating the accessibility to V(D)J recombinase. Acetylation of the H3 and H4 histones spanning the D_H–J_H regions occurs during D_H to J_H rearrangement, and acetylation of V_H histones occurs during V_H to DJ_H rearrangement (34). However, V_H histones are deactylated during the transition to the pre–B cell stage, in part as a result of a loss of IL-7 signaling (35). H3 and H4 acetylation at the *Igk* locus appears to originate at the pro–B cell stage (36, 37) but increases substantially in pre–B cells (37). Enhancer elements may contribute to the chromatin remodeling events by recruiting histone modifiers to the Ig loci (38). Overexpression of E2A is sufficient to activate *Igk* rearrangement likely through its direct binding to the *Igk* intronic enhancer (39, 40) and V_κ promoters (41). In addition, E2A has been shown to interact with multiple histone acetyltransferase complexes (42–44).

Because enhancers are important in activating V(D)J rearrangement, we hypothesized that Eμ might be involved in this developmental stage-specific process. To test this hypothesis, we replaced the endogenous MiE_κ with Eμ in mice.

RESULTS

Generation of EμR mice

To replace the endogenous *Igk* intronic enhancer with the heavy chain intronic enhancer (Eμ), the 0.8-kb XbaI fragment spanning the entire Eμ element and flanking MAR sequences was inserted 5′ of a *lox*P-flanked phosphoglycerol kinase (PGK)–*Neo*^{r} gene (f-PGK-*Neo*^{r}). This enhancer replacement cassette was placed into a targeting vector that was used previously to delete *Igk* intronic enhancer (Fig. 1 B; reference 21). Homologous recombination was confirmed by Southern blotting with EcoRI digestion of genomic DNA and hybridization to probe A (Fig. 1, A, C, and E). To remove the neomycin resistance gene from the targeted allele, heterozygous mutant embryonic stem (ES) cells were transiently transfected with a plasmid that drives the expression of the *Cre* recombinase. Deletion of the *Neo*^{r} gene in subcloned ES cells was confirmed by Southern blotting with EcoRI digestion and hybridization to probe A (Fig. 1, A, D, and E). PGK-*Neo*^{r}–deleted ES clones were used to generate chimeric animals that transmitted the EμR mutation into mouse germline.

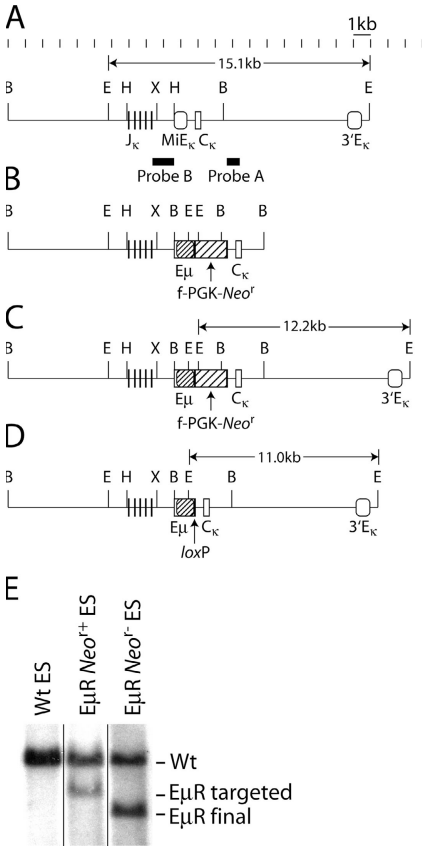

Figure 1. Generation of EμR knockin ES cells and mice. (A) Endogenous germline *Igk* locus. The lengths of the diagnostic restriction fragments and probes are shown. Markings above the diagram are spaced at 1-kb intervals. All maps are to scale. (B) Targeting construct to replace MiE_κ with Eμ (striped rounded box) and floxed PGK-*Neo*^{r} (f-PGK-*Neo*^{r}; striped box). (C) Targeted locus with f-PGK-*Neo*^{r} inserted. The size of the mutant EcoRI restriction fragment is shown. (D) Knockin allele with f-PGK-*Neo*^{r} removed by *Cre*/*lox*P-mediated deletion. (E) Southern blotting analysis of ES cell genomic DNA digested with EcoRI and probed with probe A. First lane, WT ES cell DNA; second lane, heterozygous EμR ES cell with PGK-*Neo*^{r} inserted; third lane, heterozygous EμR knockin with PGK-*Neo*^{r} deleted. Bands corresponding to the WT, EμR with PGK-*Neo*^{r} inserted, and knockin alleles are indicated on the right. B, BamHI; E, EcoRI; H, HindIII; X, XbaI.

EμR mice exhibit moderate defects in κ^+ B cell development

To determine the effects of the EμR mutation on B cell development, BM and spleen cells derived from WT and EμR mice were analyzed by flow cytometry. In spleens from EμR mice, we found an ∼50% decrease in the total number of B cells compared with WT controls (Fig. 2 C). The percentage of κ^+ splenic B cells was reduced, lowering the κ/λ ratio from 20:1 in WT mice to 6:1 in EμR mice (Fig. 2, B and D). These data indicate an impairment in the development of κ^+ B cells. This defect is not caused by impaired *Igk* expression because both the surface expression and transcription of *Igk* were identical between WT and EμR splenic κ^+ B cells (Fig. 2, E and F).

Consistent with the reduction of B cells in the spleen, a moderate increase in the percentage of pre–B cells ($B220^+CD43^-IgM^-$) and a decrease in immature B cells ($B220^+IgM^+IgD^{low}$) was detected in EμR BM compared with those in WT controls (Fig. 3, A–C). Because the percentage of pro–B cells was similar between WT and EμR BM, these data indicate that the defect in EμR B cell development originates at the pre–B cell stage, where *Igk*

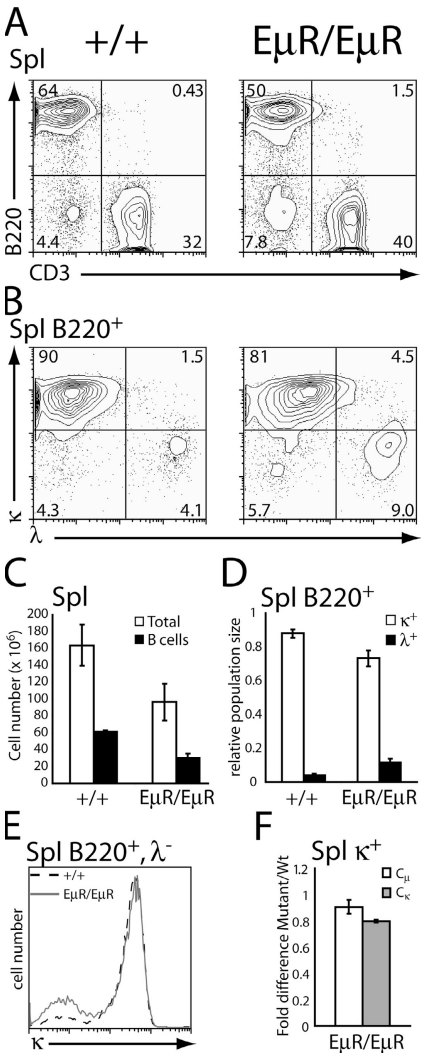

Figure 2. Analysis of splenic B cells in WT and EμR 5–8-wk-old littermates. (A) Flow cytometric analysis of B cells ($B220^+$) and T cells ($CD3^+$) in the spleens of WT and EμR mice. The genotypes are indicated at the top. Live cells (propidium iodide$^-$) within the lymphoid gate are shown. (B) κ/λ ratio of splenic $B220^+$ cells. (A and B) Percentages of total cells within each quadrant are shown. (C) B cell counts in 1-mo-old WT and EμR spleens. Absolute numbers of total white blood cells (white bars) and B cells (black bars) are shown with error bars (SD; $n = 4$). (D) Proportions of splenic κ^+ (white bars) and λ^+ (black bars) B cells shown with error bars (SD; $n = 5$). (E) κ surface expression in WT (dashed line) and EμR (solid gray line) $B220^+$, λ^- splenic lymphocytes. (F) Analysis of κ mRNA levels in κ^+ splenic B cells by quantitative real-time PCR. The κ mRNA levels were normalized to GAPDH mRNA levels. The ratio of mRNA levels of Cμ and C_κ in EμR B cells relative to WT are shown with error bars (SD; $n = 2$).

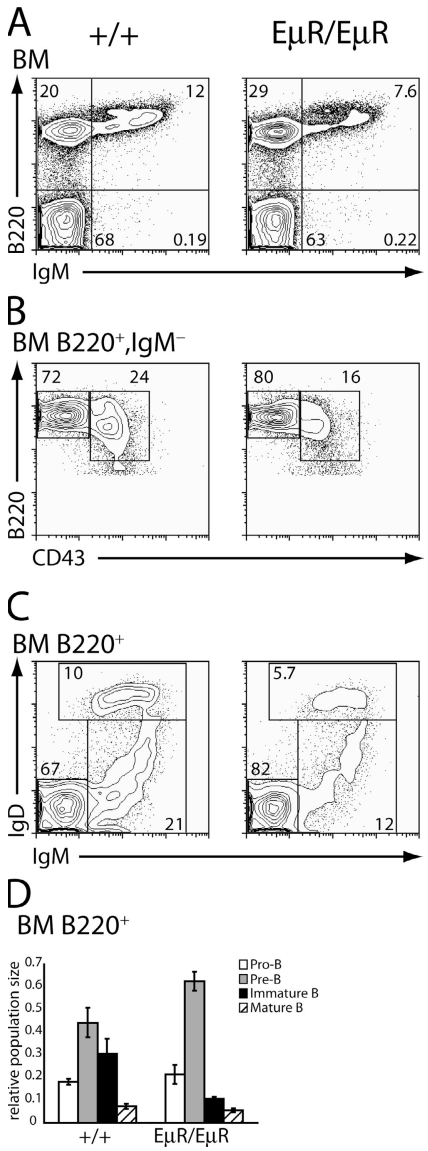

Figure 3. Analysis of BM B cell populations. (A) Flow cytometric analysis of BM from WT and EμR mice. Percentages of total cells within each quadrant are shown. Genotypes are indicated above each blot. (B) BM pro- and pre-B cell population. Only $B220^+$, IgM^- cells within the lymphocyte gate are shown. (C) BM cells were stained with anti-B220, anti-IgM, and anti-IgD antibodies. Only $B220^+$ cells are shown. Gates for pro-/pre-B cells ($B220^+/IgM^-/IgD^-$), immature B cells ($B220^+/IgM^+/IgD^{-,lo}$), and mature B cells ($B220^+/IgM^+/IgD^{hi}$) are indicated. The percentages of total cells within the lymphoid gate are shown. (D) Statistical analysis of the populations of B lineage cells in the BM of 5–8-wk-old WT and EμR littermates (error bars represent SD; $n = 2$).

normally rearranges (Fig. 3 D). This partial developmental block is similar to that observed in $MiE_\kappa^{-/-}$ mice (Fig. S1, A, B, and E; available at http://www.jem.org/cgi/content/full/jem.20052310/DC1). However, $MiE_\kappa^{-/-}$ mice have a much more severe decrease in the κ/λ ratio in splenic B cells than that observed in EμR mice (Fig. S1, B and F).

To directly compare the overall rearrangement efficiency of the EμR and WT allele, we bred EμR mice with knockin mice with their mouse κ constant region (mC_κ) replaced with the human κ constant region (hC_κ; Fig. S2 A, available at http://www.jem.org/cgi/content/full/jem.20052310/DC1). Analysis of $+/hC_\kappa$ and $E\mu R/hC_\kappa$ mice showed that they had similar populations of B cells in BM

(Fig. S2 B). In the spleen, +/hC$_\kappa$ mice had approximately equal numbers of hC$_\kappa^+$ and mC$_\kappa^+$ B cells (Fig. S2, C and D). However, EμR/hC$_\kappa$ mice had a dramatic reduction in the percentage of mC$_\kappa^+$ B cells with a ratio of hC$_\kappa^+$/mC$_\kappa^+$ B cells of ~6:1 (Fig. S2, C and D). Therefore, the overall efficiency of the EμR allele appears to be lower than that of the WT allele.

Igk rearrangement is activated by EμR in pro–B cells

To examine whether EμR affects the timing of V(D)J recombination, we used a PCR assay to analyze *Igk* rearrangement in WT and EμR homozygous pro– and pre–B cells (Fig. 4 A). The degenerate V$_\kappa$ primer (V$_\kappa$D), which binds to ~90% of V$_\kappa$ gene segments, was used together with a primer downstream of J$_\kappa$5 (primer MAR35; reference 26). Consistent with previous studies, a very low level of *Igk* rearrangement was detected in WT pro–B cells (Fig. 4 B, left; references 45, 46). However, rearrangement of the EμR allele is dramatically increased (~16-fold) in the pro–B cells of EμR mice (Fig. 4, B and C). At the pre–B cell stage, the levels of *Igk* rearrangement were similar between the WT and EμR mice (Fig. 4 B, right).

To estimate the level of rearrangement of EμR allele in pro–B cells, we designed a real-time PCR assay using primers that flanked the J$_\kappa$1 gene segment and its recombination signal sequence (RSS) to analyze the level of unrearranged *Igk* allele in pro–B cells (Fig. 4 D, top). As this PCR reaction cannot amplify the majority of rearranged *Igk* alleles in pre–B

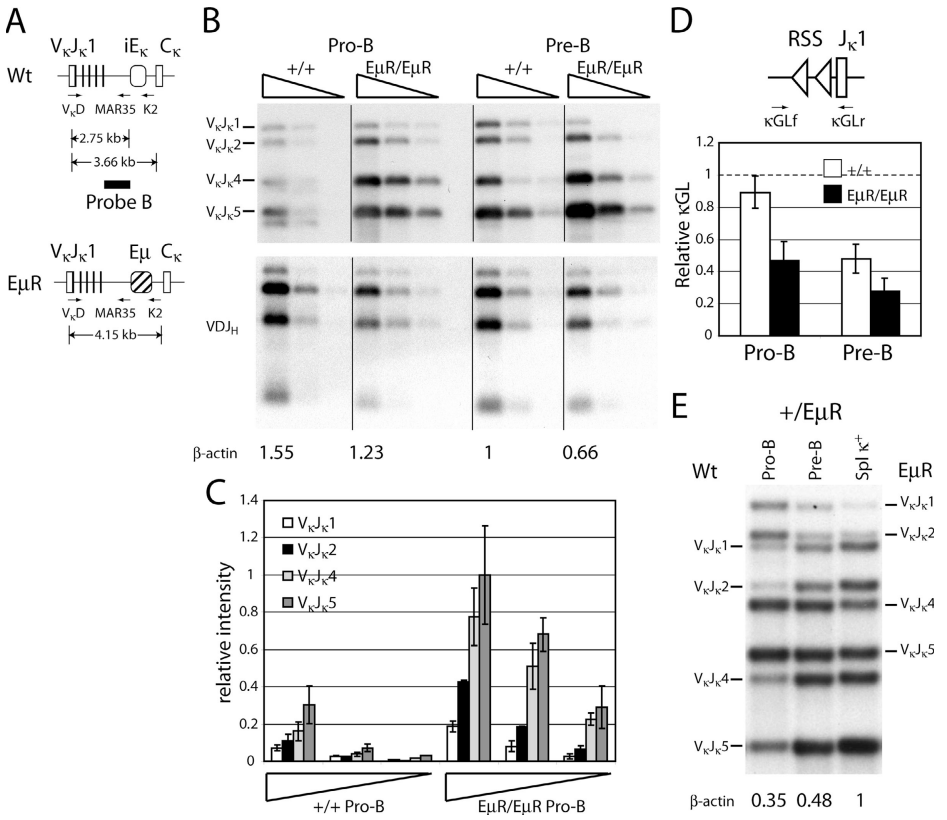

Figure 4. *Igk* rearrangement in +/+, EμR/EμR, and +/EμR mice. (A) PCR strategy to detect *Igk* rearrangement. Configuration of the rearranged *Igk* locus in WT and EμR B lineage cells. Location of the PCR primers and probe and the size of the PCR product for a V$_\kappa$ to J$_\kappa$1 rearrangement are shown. (B) Semiquantitative PCR analysis of *Igk* rearrangement using primers V$_\kappa$D and MAR35 in the pro– and pre–B cells of WT and EμR mice. Genomic DNA was serially diluted fourfold. Bands corresponding to the rearrangement of V$_\kappa$ to each of the four J$_\kappa$ gene segments are indicated on the left. To control for the amount of genomic DNA used for PCR analysis, rearrangement of the *IgH* locus (VDJ$_H$) is shown in the bottom panel. The relative amount of genomic DNA used for the PCR reaction was determined by quantitative real-time PCR analysis of the β-actin gene and is shown at the bottom. (C) Quantitative analysis of *Igk* rearrangement in pro–B cells. The intensity of each amplified product of V$_\kappa$J$_\kappa$ rearrangement is normalized to the intensity of VDJ$_H$ rearrangement. (D) Percentage of unrearranged *Igk* alleles (κGL) in WT and EμR pro– and pre–B cells. The primer annealing locations for the forward (κGLf) and reverse (κGLr) primers are shown. κGL levels were normalized to the levels of the β-actin genomic region. The percentage is calculated by dividing the κGL levels in +/+ or EμR/EμR pre–B cells by those in ES cells. Error bars represent SD. (E) PCR amplification of rearranged *Igk* alleles in sorted heterozygous (+/EμR) B lineage cells. Genomic DNA from sorted pro–, pre–, and mature B cells was amplified with the degenerate V$_\kappa$ primer and primer K2. Bands corresponding to the rearrangements of V$_\kappa$ to each of the four J$_\kappa$ gene segments of the WT allele and EμR allele are indicated. The relative amount of genomic DNA used for the PCR reaction is shown at the bottom.

cells, it allowed us to estimate the proportion of unrearranged *Igk* loci using genomic DNA from the nonrearranging ES cells as a control. Based on this assay, it was estimated that ~90 and 50% of *Igk* alleles were unrearranged in WT and EμR pro–B cells, respectively, indicating substantial *Igk* rearrangement in EμR pro–B cells (Fig. 4 D). In addition, it was estimated that ~50% of WT *Igk* alleles were unrearranged in pre–B cells, whereas ~30% of EμR alleles were unrearranged (Fig. 4 D).

To further compare *Igk* rearrangement efficiency between the WT and EμR alleles, we analyzed *Igk* rearrangement in pro–, pre–, and mature κ^+ B cells derived from heterozygous (+/EμR) mice using primers $V_\kappa D$ and K2 (Fig. 4 E). The small size difference between the PCR products amplified from the rearranged WT and EμR *Igk* alleles allowed the direct comparison of the two alleles in the same reaction (Fig. 4 A). Consistent with the notion that rearrangement of the EμR allele is activated in pro–B cells, the levels of $V_\kappa J_{\kappa 1–5}$ rearrangement of the EμR allele were considerably increased when compared with those of the WT allele in +/EμR pro–B cells (Fig. 4 E, left lane). However, in +/EμR pre–B cells, $V_\kappa J_{\kappa 1–5}$ rearrangements of the WT allele were increased compared with those of the EμR allele (Fig. 4 E, middle lane), and, in splenic κ^+ B cells, $V_\kappa J_{\kappa 1–5}$ rearrangements of the WT allele appeared to surpass those of the EμR allele (Fig. 4 E, right lane). This trend of increasing contribution of the WT allele and decreasing contribution of the EμR allele at later stages of development suggests that the overall rearrangement of the EμR allele is less efficient than WT in pre–B cells and beyond.

EμR does not support *Igk* rearrangement in pre–B cells

Productive rearrangement of the *Igk* allele in EμR pro–B cells would lead to IgM surface expression and direct transition to the immature B cell stage, whereas EμR pro–B cells with nonproductive *Igk* rearrangements would differentiate into pre–B cells. If this hypothesis is true, the rearrangements detected in EμR pre–B cells could be nonproductive ones that originated at the pro–B cell stage. To identify the origin of the EμR rearrangements detected in pre–B cells, we took advantage of the finding that terminal deoxynucleotidyl transferase is expressed exclusively in pro–B cells and mediates the nontemplated insertion of nucleotides, called N nucleotides, into the junctions of V, D, and J gene segments (47, 48). Because terminal deoxynucleotidyl transferase is not expressed in pre–B cells, N-nucleotide insertions rarely occur in $V_\kappa J_\kappa$ junctions of WT B cells and can be regarded as a hallmark of V(D)J rearrangements that occurred at the pro–B cell stage. We amplified and sequenced $V_\kappa J_\kappa 1$ junctions from EμR pro–, pre–, and mature B cells as well as from WT pre–B cells (Fig. 5 A). This analysis showed that 78% of $V_\kappa J_\kappa 1$ junctions in EμR pro–B cells contained N nucleotides. Similarly, 67% of $V_\kappa J_\kappa 1$ junctions in EμR pre–B cells contained N nucleotides in contrast to the 10% of $V_\kappa J_\kappa 1$ junctions in WT pre–B cells that contained N nucleotides. In addition, $V_\kappa J_\kappa 1$ rearrangements observed in EμR pre–B cells were

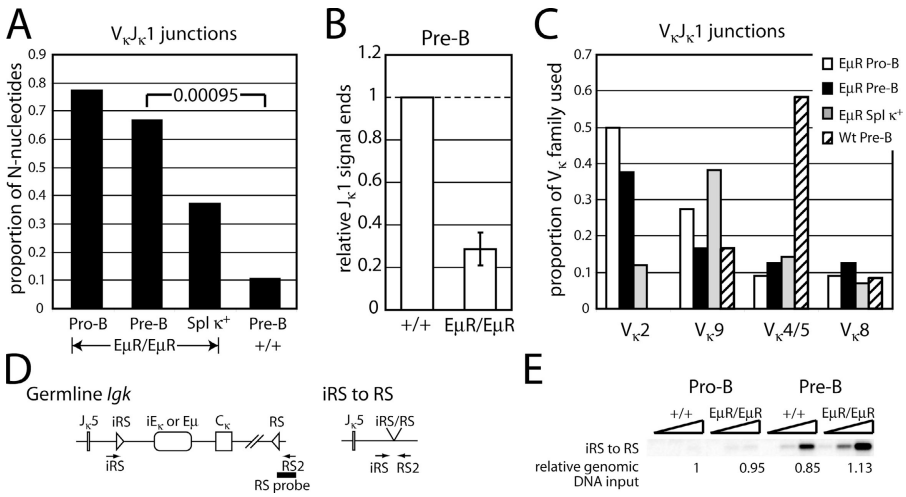

Figure 5. Analysis of $V_\kappa J_\kappa$ junctions and RS recombination in WT and EμR B cells. (A) Percentages of total $V_\kappa J_\kappa 1$ junctions with N-nucleotide insertions in sorted pro–, pre–, and mature B cells of WT and EμR mice. The number of sequences analyzed for EμR pro–, EμR pre–, EμR spleen κ^+, and WT pre–B cells are 22, 24, 43, and 12, respectively. P values for the comparison of N nucleotides in EμR pre–B cell populations to that of WT pre–B cells are shown (two-tailed paired Student's *t* test). (B) Detection of pre–B cell rearrangements by real-time LM-PCR of $J_\kappa 1$ SE breaks in WT and EμR pre–B cells. Samples were normalized to the β-actin locus. SEs detected in EμR pre–B cells are shown relative to WT. Error bar represents SD. (C) Proportions of several V_κ family members used in the $V_\kappa J_\kappa 1$ rearrangements in the pro–, pre–, and splenic κ^+ B cells of EμR mice as well as WT pre–B cells. The four most commonly used V_κ families are shown. (D and E) Analysis of RS rearrangement in WT and EμR pro– and pre–B cells. (D) Diagram of PCR strategy. Only alleles that have undergone rearrangement between the iRS and RS sequences will amplify. (E) Genomic DNA was serially diluted fivefold and amplified with the iRS and RS2 primers. The relative amount of genomic DNA in the most concentrated samples of the PCR reaction was determined by quantitative real-time PCR analysis of the β-actin gene and is shown at the bottom.

almost entirely nonproductive (21 of 24 sequences out of frame), suggesting that these rearrangements represent nonproductive rearrangements carried over from the pro–B cell stage. In further support of this notion, >80% of $V_\kappa J_\kappa 5$ junctions (14 of 17 sequences) contain N nucleotides and are mostly out of frame in EμR pre–B cells (unpublished data).

To further test whether the EμR allele rearranges inefficiently in pre–B cells, we used a quantitative real-time ligation-mediated (LM) PCR assay to determine the level of the signal end (SE) double-strand breaks, a hallmark of RAG-induced cleavage, at the $J_\kappa 1$ gene segment in WT and EμR pre–B cells as described previously (49). Compared with that in WT pre–B cells, the level of $J_\kappa 1$ SE breaks was reduced by approximately fourfold in EμR pre–B cells (Fig. 5 B). Considering that the level of unrearranged *Igk* alleles in EμR pre–B cells was 60% of that in WT pre–B cells (Fig. 4 D), this suggested that the rearrangement frequency of the EμR allele was only ∼40% of that of the WT *Igk* allele in pre–B cells. Because a similar defect in *Igk* rearrangement was observed in MiE_κ-deleted mice, these findings indicate that Eμ cannot functionally replace MiE_κ to support V(D)J rearrangement in pre–B cells.

Despite the high frequency of N-nucleotide insertions in $V_\kappa J_\kappa 1$ in EμR pro– and pre–B cells, only 37% of $V_\kappa J_\kappa 1$ rearrangements from splenic κ^+ B cells contained N nucleotides (Fig. 5 A), suggesting that pro–B cell–derived rearrangements

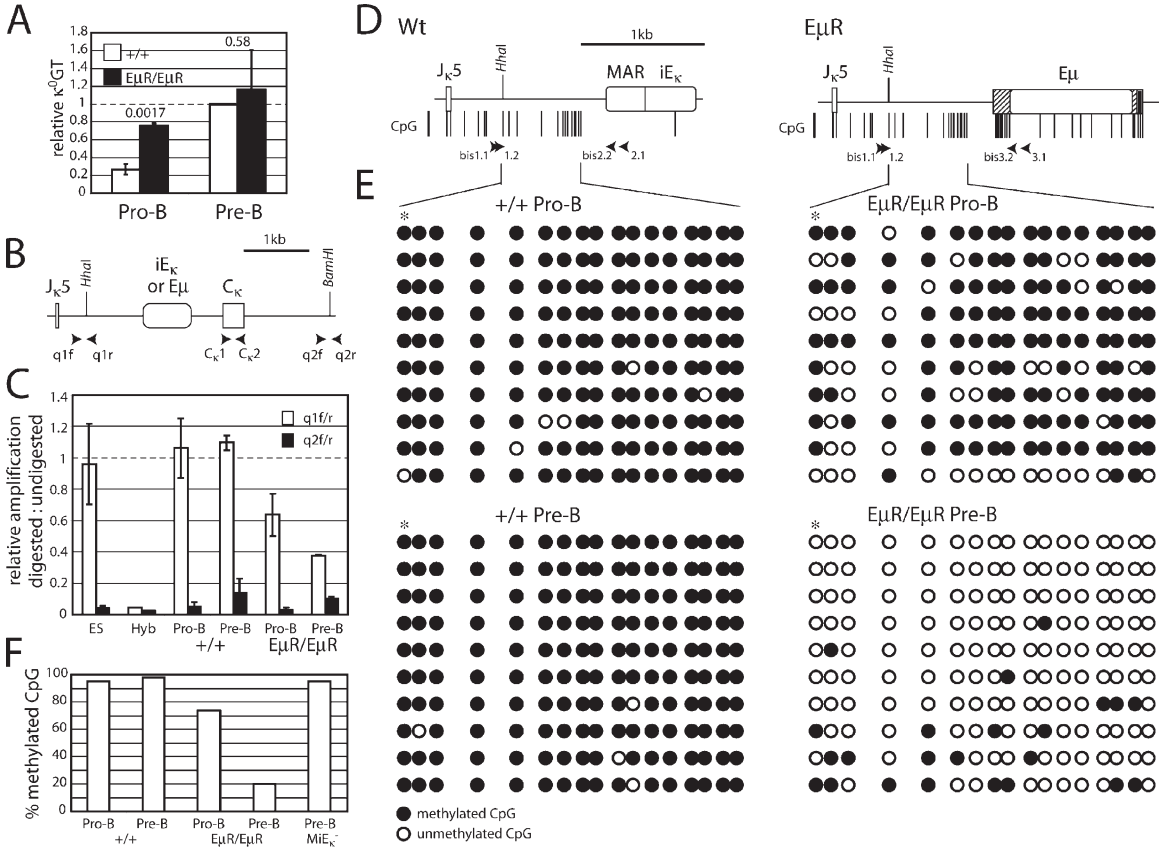

Figure 6. Analysis of accessibility of the JC_κ region in WT and EμR pro– and pre–B cells. (A) Relative κ^0GT expression in sorted pro– (left) and pre–B cells (right) of WT and EμR mice. κ^0GT mRNA levels were normalized to the levels of β-actin mRNA. The κ^0GT levels of all samples are relative to those in WT pre–B cells. P values, which are shown in each graph, were generated using the two-tailed paired Student's *t* test (error bars represent SD; $n = 3$). (B) MSRE-QPCR strategy. Restriction sites and primer annealing locations are shown. (C) MSRE-QPCR analysis of genomic DNA derived from pro– and pre–B cells of WT and EμR mice. Genomic DNA derived from ES cells and a hybridoma line (Hyb) was used as negative and positive controls. The ratio of the amplified products from the sample digested with HhaI versus those from the undigested sample is shown. The DNA amount used for PCR was normalized by the amplification of C_κ (primers $C_\kappa 1$ and $C_\kappa 2$). (D) CpG map in the $J_\kappa C_\kappa$ intron. Locations of the CpG dinucleotides are indicated by vertical lines below the map. Primers used to amplify bisulfite-treated DNA are indicated by arrowheads. (E) Methylation status of the 17 CpG dinucleotides within the $J_\kappa C_\kappa$ intron in the pro– and pre–B cells of WT and EμR mice. Each row of circles represents the methylation status of a single PCR product (one allele). 10 representative sequences from each sample are shown. The first circle (denoted by an asterisk) corresponds to the CpG site within the HhaI restriction site that was analyzed by MSRE-QPCR. (F) Percentage of the methylated CpG sites analyzed by bisulfite genomic sequencing. Percentages were calculated as the total number of methylated CpG sites divided by the total number of CpG sites analyzed. Bisulfite analysis of MiE_κ-deleted loci is shown in Fig. S3 (available at http://www.jem.org/cgi/content/full/jem.20052310/DC1).

may be negatively selected during development and, additionally, that some rearrangement can occur beyond the pro–B and pre–B cell stages in EμR B cells. Recent studies suggest that 25–50% of mature B cells may have undergone receptor editing (50–52), a process by which recombination in light chain genes is reactivated to remove autoreactive antibodies (53–55). Therefore, it is likely that EμR B cells also undergo robust receptor editing. We analyzed V_κ usage in B cells at various developmental stages in EμR mice and WT mice and found that $V_\kappa 2$ family members were used frequently in $V_\kappa J_\kappa 1$ rearrangements in EμR pro– and pre–B cells (50 and 37%, respectively) but less frequently in splenic B cells (12%). This is consistent with a change in the B cell repertoire between BM and peripheral B cells (Fig. 5 C).

Recombining sequence (RS) rearrangement between an RSS within the $J_\kappa C_\kappa$ intron (iRS) and the RS sequence 21 kb downstream of C_κ is a primary mechanism for the receptor editing of *Igk* (56). To directly test whether EμR B cells actively undergo receptor editing of *Igk*, we analyzed the frequency of RS recombination in EμR and WT pro– and pre–B cells using a semiquantitative PCR assay as previously described (Fig. 5 D; reference 56). Although little RS rearrangement was detected in WT and EμR pro–B cells, RS recombination was increased in EμR pre–B cells when compared with that in WT pre–B cells, which is consistent with the findings that the Jκ region is accessible in EμR pre–B cells (Fig. 5 E).

The J_κ region becomes accessible in EμR pro–B cells and remains so in pre–B cells

To understand the mechanisms by which EμR activates *Igk* rearrangement at the pro–B cell stage, we analyzed κ germline transcription in pro– and pre–B cells sorted from WT and EμR BM. A real-time quantitative PCR strategy was designed to determine the amount of GT initiating from promoters upstream of the J_κ gene segments (κ^0GT) using primers immediately upstream of $J_\kappa 1$ and within the C_κ exon. mRNA levels of β-actin were also analyzed by quantitative PCR and used as the control for the input RNA amount. Consistent with increased accessibility of *Igk* loci in EμR pro–B cells, our analysis indicated an approximate threefold increase in the amount of κ^0 transcripts in EμR pro–B cells when compared with WT pro–B cells (Fig. 6 A).The amount of κ^0 transcript in EμR pre–B cells was similar to that in WT pre–B cells, suggesting that the *Igk* locus remains in an open configuration at the J_κ region in EμR pre–B cells (Fig. 6 A).

Chromatin remodeling, including DNA demethylation, modulates the accessibility of Ig gene loci to the V(D)J recombinase (31, 57). Therefore, we compared the extent of DNA methylation at the *Igk* locus within the region spanning the J_κ and C_κ exons ($J_\kappa C_\kappa$ intron) in EμR and WT pro– and pre–B cells. The methylation status at an HhaI site residing within the $J_\kappa C_\kappa$ intron just downstream of the $J_\kappa 5$ gene segment has been frequently analyzed as an indicator of the methylation status of the $J_\kappa C_\kappa$ region (Fig. 6 B; references 32, 37, 58). We designed a quantitative real-time PCR assay to detect the amount of DNA that was not cut at the HhaI site (methylated) using primers that flank that site (q1f and q1r) and compared it with undigested controls (Fig. 6 B). Consistent with previous findings, our analysis indicated little demethylation in the pro– or pre–B cells of WT mice (Fig. 6 C; reference 32). In contrast, $J_\kappa C_\kappa$ demethylation was substantially increased in the pro–B cells of EμR mice (Fig. 6 C). More strikingly, the majority of *Igk* loci appeared to be demethylated in the EμR pre–B cells (Fig. 6 C). Therefore, this assay demonstrates that Eμ has the ability to induce demethylation of the $J_\kappa C_\kappa$ region in pro– and pre–B cells.

To confirm that the notable differences in methylation observed at the HhaI site are representative of the entire $J_\kappa C_\kappa$ region, we analyzed the methylation status of adjacent CpG sites using bisulfite genomic sequencing (59). Consistent with the methylation-sensitive restriction enzyme real-time quantitative PCR (MSRE-QPCR) assay, in WT pro– and pre–B cells, *Igk* loci were hypermethylated at nearly all CpG sites examined (Fig. 6, B and E). In EμR pro–B cells, *Igk* loci were partially demethylated with a mean of 25% (Fig. 6, E and F). This pattern is distinct from the monoallelic demethylation pattern of *Igk* loci observed in WT splenic B cells, where normally one allele is fully methylated and the other allele is fully demethylated (23, 32). In EμR pre–B cells, the $J_\kappa C_\kappa$ region was highly demethylated with a mean of 14.3 of 17 sites (86%) unmethylated per sequence (Fig. 6, E and F).

We have previously observed the hypomethylation of *Igk* loci in mature splenic $MiE_\kappa^{-/-}$ B cells, suggesting the possibility that the hypomethylation observed in EμR loci is caused by the absence of MiE_κ (23). However, similar to the WT allele, the MiE_κ-deleted *Igk* locus is mostly methylated in pre–B cells (Fig. S3, available at http://www.jem.org/cgi/content/full/jem.20052310/DC1). Thus, the hypomethylation of the EμR locus is caused by the presence of Eμ, not the absence of MiE_κ. In conclusion, our findings indicate that Eμ can promote robust chromatin remodeling of the $J_\kappa C_\kappa$ region in both pro– and pre–B cells.

The V_κ regions are accessible in EμR pro–B cells, but not in pre–B cells

V(D)J recombination requires that both the V region and (D)J region are accessible to the recombination machinery. Because V_κ germline transcription (V_κGT) predicts their accessibility to V(D)J recombinase (1), we examined germline transcription of five V_κ gene segments that spread throughout the locus in EμR pro– and pre–B cells (Fig. 7 A). The amount of V_κGT was quantitated by real-time PCR using primers annealing to the transcribed regions downstream of the V_κ RSS, which are deleted upon rearrangement and, thus, only amplify transcription from unrearranged V_κ promoters (Fig. 7 B). In pooled EμR pro–B cells, the V_κ germline transcription of three of five V_κ genes was increased in EμR pro–B cells when compared with WT pro–B cells (Fig. 7 C). Thus, consistent with the increased rearrangement of the EμR allele in pro–B cells, EμR appears to increase the accessibility of V_κ genes in pro–B cells.

To understand the basis for the inefficient *Igk* rearrangement observed in EμR pre–B cells, we also analyzed germline transcription of five V_κ segments in EμR pre–B cells. Because the percentage of V_κ in germline configuration is likely to be different between WT and EμR pre–B cells, the ratio of the amount of each germline V_κ in EμR pre–B cells versus WT pre–B cells was analyzed by quantitative real-time PCR using primers that are specific to each unrearranged V_κ (Fig. 7 E). By normalizing the levels of V_κGT to the amount of germline V_κ, germline transcription of four of the five V_κ genes examined was markedly reduced in EμR pre–B cells when compared with that in WT pre–B cells, suggesting a reduced V_κ accessibility in EμR pre–B cells (Fig. 7 D).

Histone acetylation is another hallmark for accessibility to the V(D)J recombinase (38). Therefore, we also examined histone acetylation of V_κ segments in pooled WT and EμR pre–B cells by chromatin immunoprecipitation (ChIP) assays using an antibody against acetylated histone H3. To specifically detect only germline V_κ gene segments, we used the same primer sets that were used to analyze V_κGT to determine the amount of germline V_κ in both immunoprecipitated chromatin and total input chromatin. In pooled pre–B cells sorted from five EμR and five age-matched WT littermates, histone acetylation of the analyzed V_κ gene segments was generally reduced (Fig. 7 F). As a control, we also examined acetylation at the C_κ exon and found equivalent levels of acetylation between EμR and WT pre–B cells, which is consistent with the observation that the $J_\kappa C_\kappa$ region remains open in pre–B cells (Fig. 7 F). Together with the reduction in V_κGT, these data indicate that the inefficient *Igk* rearrangement observed in EμR pre–B cells is caused by the reduced accessibility of V_κ regions to the V(D)J recombinase.

The reduction in V_κ accessibility observed in EμR pre–B cells could be caused by the presence of Eμ and/or the absence of MiE_κ. To distinguish between these possibilities, we analyzed V_κ germline transcription in pre–B cells sorted from $MiE_\kappa^{-/-}$ mice. Germline transcription of most V_κ genes analyzed was considerably reduced in $MiE_\kappa^{-/-}$ pre–B cells compared with that in WT pre–B cells, indicating that MiE_κ is required for the accessibility of V_κ in pre–B cells (Fig. 7 G). In contrast to that in EμR pre–B cells, κ^0GT was dramatically reduced in $MiE_\kappa^{-/-}$ pre–B cells (Fig. 7 G). V_κGT was normal in $3'E_\kappa^{-/-}$ pre–B cells, but, consistent with previous studies (22, 23), κ^0GT was reduced (Fig. 7 H). Therefore, MiE_κ plays an important role in promoting the accessibility of both V_κ and J_κ regions in pre–B cells, and Eμ can compensate for MiE_κ in opening up the J_κ region but not the V_κ region in EμR pre–B cells.

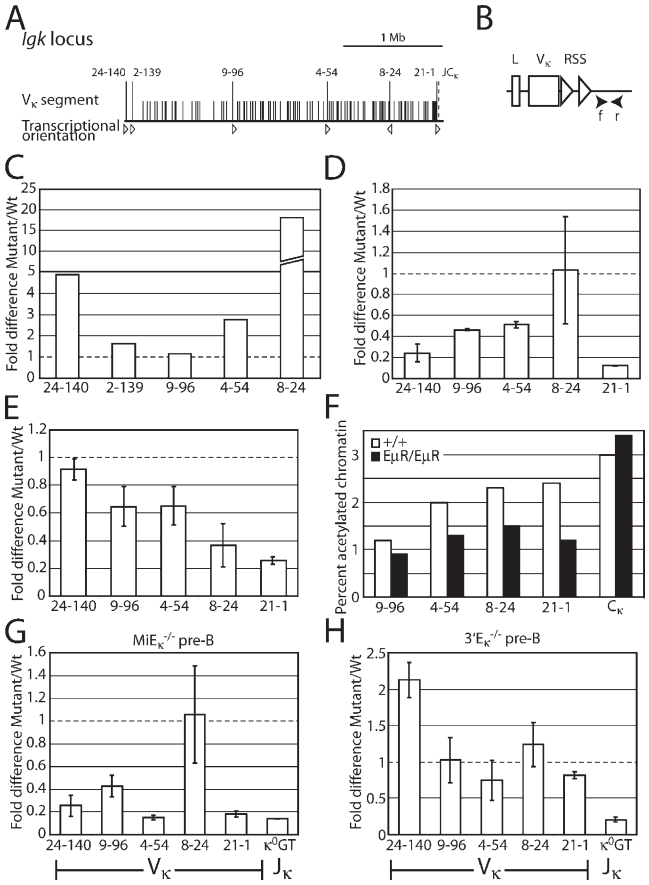

Figure 7. Analysis of V_κ gene accessibility in *Igk* mutant mice. (A) Map of *Igk* locus. Locations of V_κ genes are represented by vertical lines. The six V_κ genes analyzed are labeled above and are represented with longer lines. The transcriptional orientation of each of the six V_κ genes is indicated by arrowheads below. The JC_κ region is represented by a broken line. (B) Real-time PCR strategy to quantitate the amount of V_κ germline transcription (V_κGT). A generic map of unrearranged V_κ gene segment is shown with leader (L) and V_κ exons (boxes) and the RSS sequence (triangles). Forward (f) and reverse (r) primers are indicated by arrowheads. (C) V_κ germline transcription (V_κGT) in pooled WT and EμR pro–B cells. The amount of GTs of five V_κ genes was analyzed by quantitative real-time PCR and normalized to CD19 mRNA levels. The thick horizontal line at the relative V_κGT value of five indicates a change in scale. (D) V_κGT in WT and EμR pre–B cells. All V_κGT levels were normalized to the levels of CD19 mRNA and the relative amount of unrearranged V_κ alleles in EμR pre–B cells versus that in WT pre–B cells, as shown in E. (C and D) The y axis represents the ratio of V_κGT in EμR pro–/pre–B cells versus that in WT pro–/pre–B cells. Error bars represent SD. (F) Histone acetylation of V_κ in pools of WT and EμR pre–B cells analyzed by ChIP. The V regions analyzed are labeled on the x axis, and the percentage of chromatin immunoprecipitated from the total input chromatin is shown on the y axis. The primers used for the V_κ genes are the same as those used for the V_κGT analysis, and the C_κ primers are the same as used in Fig. 5 B. (G and H) Germline transcription of V_κ and J_κ regions in $MiE_\kappa^{-/-}$ (G) and $3'E_\kappa^{-/-}$ (H) pre–B cells. The ratio of the GT levels in mutant pre–B cells versus those in WT pre–B cells is shown on the y axis.

DISCUSSION

It has been well established that V(D)J recombination of the Ig heavy and light chain genes occur in a sequential manner (1). In this context, the rearrangement of *IgH* chain genes occurs exclusively in pro–B cells, whereas the rearrangement of *IgL* chain genes occurs primarily in pre–B cells. Our findings indicate that EμR replacement greatly increases *Igk*

rearrangement in pro–B cells. In addition, the germline transcription of both V_κ and J_κ regions as well as DNA demethylation at the J_κ region are substantially increased in EμR pro–B cells, indicating that Eμ is sufficient to promote the accessibility of these loci to V(D)J recombinase and activate V(D)J recombination in pro–B cells.

To maintain the sequential rearrangement of *IgH* and *IgL* chain genes, the rearrangement of *IgH* loci occurs in pro–B cells but not in pre–B cells. Analysis of B cell development and *Igk* rearrangement suggests that *Igk* rearrangement is not efficient in EμR pre–B cells. In further support of this notion, the percentage of $V_\kappa J_\kappa$ junctions containing N nucleotides is similar in EμR pro–B and pre–B cells, indicating that the majority of the *Igk* rearrangements detected in EμR pre–B cells have occurred in pro–B cells. In addition, the level of RAG-induced SE breaks is markedly reduced in EμR pre–B cells. Therefore, Eμ promotes V(D)J recombination in pro–B cells but cannot support efficient V(D)J rearrangement in pre–B cells, further implicating its importance in maintaining the sequential rearrangement of *IgH* and *IgL* chain genes.

Efficient V(D)J recombination requires that both V and J regions are accessible to the V(D)J recombinase. Because the germline transcription and histone acetylation through J_κ is normal in EμR pre–B cells, the inefficient rearrangement of the EμR allele in pre–B cells is not caused by the inaccessibility of the J_κ region to the V(D)J recombinase. In contrast, germline transcription and histone acetylation of unrearranged V_κ gene segments are noticeably reduced in EμR pre–B cells, indicating that accessibility of the V_κ region is reduced in EμR pre–B cells. This scenario is remarkably similar to the *IgH* locus in normal pre–B cells, where the V_H region becomes inaccessible but the DJ_H region remains accessible (35). As germline transcription of V_κ and J_κ is considerably reduced in $MiE_\kappa^{-/-}$ pre–B cells, the reduced accessibility of V_κ in EμR pre–B cells is caused by the lack of MiE_κ. Therefore, Eμ and MiE_κ maintain the sequential rearrangement of the Ig loci by playing developmental stage-specific roles in promoting the chromatin remodeling at V regions.

Because Ig enhancers are essentially clusters of protein-binding sites, the function of an enhancer is dictated by the array of DNA-binding factors it recruits. A comparison of the known functional motifs within Eμ and MiE_κ shows that μA and μB sites are only present in Eμ. The binding of PU.1 and ETS family proteins to μA and μB sites promotes chromatin accessibility to endonucleases (60). In addition, although two E2A-binding E boxes, which are important for activating *Igk* rearrangement, are present in MiE_κ (40), three E2A-binding E boxes are present in Eμ (61). The unique combination of functional motifs within Eμ might account for its activities in activating V(D)J recombination in pro–B cells.

It remains unclear why Eμ cannot compensate for MiE_κ function in promoting the accessibility of V_κ regions in pre–B cells. Most of the known protein-binding sites within MiE_κ are also found in Eμ. One exception is the NF-κB–binding site. However, deletion of this site has no considerable impact on *Igk* rearrangement (40). Both MiE_κ and Eμ contain MARs that could bind to the nuclear matrix and extend the range of the action of its associated enhancers (62–65). It is possible that the MARs of Eμ and MiE_κ function differently in promoting V_κ accessibility in pre–B cells. Although neither the two MARs of Eμ nor the MAR of MiE_κ is required for rearrangement (66, 67), increased premature *Igk* rearrangement in pro–B cells has been detected in mice with a deletion of MAR of MiE_κ (67, 68). It is possible that certain unidentified elements within MiE_κ are required for promoting the accessibility of V_κ in pre–B cells. Alternatively, some elements within Eμ, such as μNR, might dominantly suppress its activity in promoting accessibility in V regions in pre–B cells (69).

Recent studies indicate that during recombination, Ig loci migrate to the nuclear center (70), where they contract (71) via DNA-looping (72, 73) mechanisms that bring distal V segments in close proximity to the enhancers (74). The ability of Eμ and MiE_κ to regulate V-region accessibility as far as 3 Mb away suggests that these enhancers may also play a role in regulating higher order chromatin modifications. Further analysis of the chromatin remodeling in EμR and $MiE_\kappa^{-/-}$ precursor B cells will help to define the functions of intronic enhancers in regulating such processes. In summary, the *IgH* and *Igk* intronic enhancers activate the sequential rearrangement of Ig loci by inducing stage-specific chromatin remodeling events in regions proximal to the enhancers and coordinate with V promoters to induce accessibility at distal V regions.

MATERIALS AND METHODS

Generation of EμR ES cells and knockin mice. Eμ was cloned into pBluescript and inserted into a targeting construct that was used previously to knockout the *Igk* intronic enhancer (21). Eμ was inserted into the SalI site upstream of the floxed neomycin resistance gene under control of the PGK promoter (f-PGK-*neo*^{r}), the same insertion site previously used to reintroduce mutant MiE_κ into the targeting construct (40). The targeting construct was linearized with PvuI and was electroporated into ES cells as described previously (75). Transfected ES cells were cultured with 300 μg/ml G418 and 1 μM gancyclovir to select for integration by homologous recombination. Positive clones were first screened by PCR and then by Southern blotting, digesting with EcoRI and probing with probe A as previously described (40). The WT locus produces a 15.1-kb fragment, whereas the targeted locus produces a 12.2-kb fragment. The floxed PGK-*neo*^{r} was removed through *Cre/lox*P-mediated deletion as described previously (21) and was screened by PCR and Southern blotting under the same conditions. The final configuration, called EμR, produces an 11.0-kb fragment. Positive clones were then subcloned and rescreened to ensure purity. EμR ES cells were injected into mouse blastocysts to produce chimeric mice, which were bred and screened for germline transmission of the EμR allele.

Cell purification and flow cytometry. BM and spleen cells were harvested in FACS buffer (3% FCS in PBS) and purified into single-cell suspensions. For total white blood cell counts, splenocytes were counted in 2% glacial acetic acid. For purification and flow cytometry, red blood cells were removed by treatment with red blood cell lysis buffer (0.15 M NH_4Cl, 1 mM $KHCO_3$, and 0.1 mM Na_2EDTA, pH 7.0) for 5 min at room temperature. 1 million cells were pretreated with 1 μg FcBlock (BD Biosciences) and stained in 100-μl reactions on ice for 15 min. If necessary, cells were washed and stained with streptavidin-coated dyes under the same conditions. Cells were resuspended in 0.5 μg/ml propidium iodide in FACS buffer to stain for dead cells. For spleen cell stains, live cells within the lymphocyte gate were analyzed. Additionally, to exclude clumped cells, only small lymphocytes were analyzed.

For BM stains, live lymphocytes and granulocytes were analyzed. Antibodies used are as follows: anti–B220-PE (BD Biosciences), anti–IgM-FITC (BD Biosciences), anti–CD43-biotin (BD Biosciences), anti–mouse Igκ-FITC (BD Biosciences), anti–mouse Igλ-biotin (BD Biosciences), anti–CD3-FITC (BD Biosciences), streptavidin-APC (eBioscience), and streptavidin-PECy5 (eBioscience). To obtain purified pro– and pre–B cells, BM was stained with B220-PE, IgM-FITC, and CD43-biotin and was washed and restained with streptavidin-PECy5. Pro–B cells ($B220^+$, IgM^-, and $CD43^+$) and pre–B cells ($B220^+$, IgM^-, and $CD43^-$) were sorted using a FACSVantage Cell Sorter (Becton Dickinson). κ^+ spleen cells were sorted by negative selection using the MACS system (Miltenyi Biotec), anti–Igλ-biotin antibodies, and anti-CD43 and anti-biotin microbeads according to the manufacturer's instructions and as previously described (40). The purity of sorted B cells was confirmed by FACS analysis. All purifications used were >95% $B220^+$.

Primer sequences. Sequences of all primers used are listed in the supplemental material (available at http://www.jem.org/cgi/content/full/jem.20052310/DC1).

Real-time quantitative RT-PCR analysis. RNA from sorted pro–, pre–, and κ^+ splenic B cells was purified using the RNAeasy Purification Kit (QIAGEN) as described previously (40). RNA was converted to cDNA using the Superscript first strand cDNA synthesis kit (Invitrogen) as described previously (40). cDNA was amplified using the 2× SYBR Green Master Mix (Applied Biosystems) in a sequence detection system (Prism 7000; ABI Biosystems). PCR results were analyzed using Prism 7000 SDS software (ABI Biosystems) and relative transcription calculated using the ΔC_t method according to the manufacturer's instructions.

Rearrangement PCR assay. DNA was purified from sorted B cell populations as described previously (23). Rearranged *Igk* alleles were amplified using the degenerate V_κ primer ($V_\kappa D$) and either primer K6 or primer MAR35 under PCR conditions that were previously described (23, 40). PCR products were run on an agarose gel, transferred to a membrane, and probed as previously described (23). Heavy chain rearrangement was amplified by PCR and analyzed by Southern blotting as previously described (40). RS rearrangement was analyzed with a PCR assay with primers iRS and a primer downstream of the RS RSS (primer R2) as previously described (56). The intensity of each band was calculated using a phosphorimager (Storm; GE Healthcare) as previously described (23).

Cloning and sequencing of $V_\kappa J_\kappa 1$ rearrangements. Rearranged *Igk* alleles were amplified using KOD Hotstart Polymerase (Calbiochem) according to the manufacturer's instructions. A degenerate V_κ primer with a BamHI restriction sequence inserted (V_κD.bam) and a primer that anneals between $J_\kappa 1$ and $J_\kappa 2$ with an EcoRI restriction sequence added (J_κ1.eco) were used. PCR products were purified using the Wizard SV PCR and Gel Clean-Up System (Promega) according to the manufacturer's instructions, digested with BamHI and EcoRI, and cloned into pBluescript. Clones were sequenced by Eton Biosciences using the T3 primer. Sequences were analyzed by IgBLAST software, which is available from the National Center for Biotechnology Information's website (http://www.ncbi.nlm.nih.gov/igblast/) to determine the V_κ gene segment used and to identify junctional insertions and deletions. N-nucleotide insertions were determined using previously described methods (48). In brief, insertions with sequences complementary to V_κ or J_κ ends were classified as P nucleotides. Insertions that could not be classified as P nucleotides were considered N nucleotides. For example, in the hypothetical sequence ACCGGCTGG, where the underlined sequences correspond to V_κ (left) and $J_\kappa 1$ (right), GGC would represent inserted nucleotides. Because the inserted GG nucleotides are complementary to the V_κ end, they would be classified as P nucleotides. The inserted C nucleotide, which is not complementary to either V_κ or J_κ ends, would be classified as an N nucleotide.

Detection of SE breaks by quantitative LM-PCR. Genomic DNA was purified from sorted pre–B cell populations as described previously (49). LM-PCR was performed essentially as described previously with all of the reagents provided by J. Curry of M. Schlissel's laboratory (University of California, Berkeley, Berkeley, CA; reference 49). In brief, 500 ng of genomic DNA was used in each ligation reaction. Quantitative real-time PCR analysis of the levels of the ligation product of $J_\kappa 1$ SE break was performed exactly as described previously (49). The amount of input genomic DNA was determined by quantitative real-time PCR with primers specific for the β-actin promoter.

MSRE-QPCR. DNA from sorted B cells was digested in a 50-μl reaction volume with 20 U EcoRI (New England Biolabs, Inc.) for 1 h at 37°C. Subsequently, 23 μl were transferred to a separate tube, and 20 U of both BamHI and HhaI were added. The original EcoRI digest and the EcoRI, BamHI, and HhaI triple digests were incubated overnight at 37°C. Restriction enzymes were inactivated by heating at 65°C for 20 min. Approximately 0.5 μl of digest product were used per well for real-time quantitative PCR.

Bisulfite genomic sequencing. DNA from sorted B cells was converted with sodium bisulfite using the EZ DNA Methylation Kit (Zymo Research) according to the manufacturer's instructions. Converted DNA was amplified in two rounds of PCR. In the first round, bis1.1 and either bis2.1 or bis3.1 primers were used in the following touchdown PCR program: a 5-min 95°C initial incubation followed by 15 cycles of 94°C for 1 min, x°C for 1 min, and 72°C for 2 min and 30 s, where x is 64°C for the first cycle and lowers 1°C per cycle. This was followed by 15 cycles of 94°C for 30 s, 50°C for 30 s, 72°C for 2 min and 30 s, and a final extension for 10 min at 72°C. 5–10% of the PCR product was used in a second round of PCR using primer bis1.2eco and either bis2.2bam or bis3.2bam and using KOD Hotstart Polymerase (Calbiochem) according to the manufacturer's protocol. The PCR program for the second round was 95°C for 2 min followed by 32 cycles of 94°C for 20 s, 55°C for 30 s, and 68°C for 2 min and 30 s. This was followed by a final extension for 10 min at 68°C. PCR products were purified using the Wizard SV Gel and PCR Clean-Up System (Promega), digested with BamHI and EcoRI, gel purified, and cloned into pBluescript. Sequencing was provided by the Cancer Center sequencing facility of the University of California, San Diego (UCSD).

ChIP. Sorted pre–B cells were pooled and fixed in 1% formaldehyde. Subsequent steps followed a previously described protocol (76) with some modifications. Fixed cells were lysed in L1 lysis buffer (50 mM Tris, pH 8.0, 2 mM EDTA, 0.1% NP-40, and 10% glycerol) supplemented with protease inhibitors. Nuclei were pelleted and resuspended in 300 μl L2 lysis buffer (50 mM Tris, pH 8.0, 0.1% SDS, and 5 mM EDTA) with protease inhibitors. Chromatin was fragmented by sonication, centrifuged, and diluted in dilution buffer (50 mM Tris, pH 8.0, 5 mM EDTA, 0.2 M NaCl, and 0.5% NP-40). After preclearing, immunoprecipitation was performed overnight at 4°C using 3 μl antiacetylated histone H3 antibody (Upstate Biotechnology). Immune complexes were collected with ssProtein A/G for 30 min and washed three times in washing buffer (20 mM Tris, pH 8.0, 0.1% SDS, 0.5 M NaCl, 2 mM EDTA, and 1% NP-40) and once in 0.5 M LiCl followed by three washes with TE buffer (10 mM Tris and 1 mM EDTA). Immune complexes were extracted three times with 100 μl of extraction buffer (TE buffer containing 2% SDS). DNA–protein cross-linking was reversed by heating at 65°C for 8 h. After proteinase K (100 μg for 2 h) digestion, DNA was extracted with phenol/chloroform and precipitated in ethanol. The UCSD Animal Subjects Committee approved all experiments that involved mice.

Online supplemental material. Fig. S1 shows the analysis of B cell populations in $MiE_\kappa^{-/-}$ BM and spleen by flow cytometry. Fig. S2 shows the analysis of B cell populations in Eμ$R \times hC_\kappa$ BM and spleen. Fig. S3 shows the analysis of methylation in $MiE_\kappa^{+/-}$ pre–B cells. Supplemental material also provides a list of all primer sequences used. Online supplemental material is available at http://www.jem.org/cgi/content/full/jem.20052310/DC1.

We thank Drs. John Curry and Mark Schlissel for all reagents for the LM-PCR assay. We also thank Drs. David Baltimore, Stephen Hedrick, Cornelis Murre, David Nemazee, and Eugene Oltz for critical reading of this manuscript.

This work was supported by a National Institutes of Health grant (AI44838) to Y. Xu.

The authors have no conflicting financial interests.

Submitted: 17 November 2005
Accepted: 19 May 2006

REFERENCES

1. Bassing, C.H., W. Swat, and F.W. Alt. 2002. The mechanism and regulation of chromosomal V(D)J recombination. *Cell*. 109:S45–S55.
2. Yancopoulos, G.D., and F.W. Alt. 1985. Developmentally controlled and tissue-specific expression of unrearranged Vh gene segments. *Cell*. 40:271–281.
3. Alt, F.W., T.K. Blackwell, and G.D. Yancopoulos. 1987. Development of the primary antibody repertoire. *Science*. 238:1079–1087.
4. Stanhope-Baker, P., K.M. Hudson, A.L. Shaffer, A. Constantinescu, and M.S. Schlissel. 1996. Cell type-specific chromatin structure determines the targeting of V(D)J recombinase activity in vitro. *Cell*. 85: 887–897.
5. Sleckman, B.P., J.R. Gorman, and F.W. Alt. 1996. Accessibility control of antigen-receptor variable-region gene assembly: role of cis-acting elements. *Annu. Rev. Immunol*. 14:459–481.
6. Hesslein, D.G., and D.G. Schatz. 2001. Factors and forces controlling V(D)J recombination. *Adv. Immunol*. 78:169–232.
7. Schlissel, M.S. 2003. Regulating antigen-receptor gene assembly. *Nat. Rev. Immunol*. 3:890–899.
8. Parslow, T.G., and D.K. Granner. 1982. Chromatin changes accompany immunoglobulin kappa gene activation: a potential control region within the gene. *Nature*. 299:449–451.
9. Emorine, L., M. Kuehl, L. Weir, P. Leder, and E.E. Max. 1983. A conserved sequence in the immunoglobulin J kappa-C kappa intron: possible enhancer element. *Nature*. 304:447–449.
10. Queen, C., and D. Baltimore. 1983. Immunoglobulin gene transcription is activated by downstream sequence elements. *Cell*. 33:741–748.
11. Gillies, S.D., S.L. Morrison, V.T. Oi, and S. Tonegawa. 1983. A tissue-specific transcription enhancer element is located in the major intron of a rearranged immunoglobulin heavy chain gene. *Cell*. 33:717–728.
12. Banerji, J., L. Olson, and W. Schaffner. 1983. A lymphocyte-specific cellular enhancer is located downstream of the joining region in immunoglobulin heavy chain genes. *Cell*. 33:729–740.
13. Meyer, K.B., and M.S. Neuberger. 1989. The immunoglobulin kappa locus contains a second, stronger B-cell-specific enhancer which is located downstream of the constant region. *EMBO J*. 8:1959–1964.
14. Liu, Z.-M., J.B. George-Raizen, S. Li, K.C. Meyers, M.Y. Chang, and W.T. Garrard. 2002. Chromatin structural analyses of the mouse Igkappa gene locus reveal new hypersensitive sites specifying a transcriptional silencer and enhancer. *J. Biol. Chem*. 277:32640–32649.
15. Pettersson, S., G.P. Cook, M. Bruggemann, G.T. Williams, and M.S. Neuberger. 1990. A second B cell-specific enhancer 3′ of the immunoglobulin heavy-chain locus. *Nature*. 344:165–168.
16. Dariavach, P., G.T. Williams, K. Campbell, S. Pettersson, and M.S. Neuberger. 1991. The mouse IgH 3′-enhancer. *Eur. J. Immunol*. 21: 1499–1504.
17. Lieberson, R., S.L. Giannini, B.K. Birshtein, and L.A. Eckhardt. 1991. An enhancer at the 3′ end of the mouse immunoglobulin heavy chain locus. *Nucleic Acids Res*. 19:933–937.
18. Chen, J., F. Young, A. Bottaro, V. Stewart, R.K. Smith, and F.W. Alt. 1993. Mutations of the intronic IgH enhancer and its flanking sequences differentially affect accessibility of the JH locus. *EMBO J*. 12:4635–4645.
19. Serwe, M., and F. Sablitzky. 1993. V(D)J recombination in B cells is impaired but not blocked by targeted deletion of the immunoglobulin heavy chain intron enhancer. *EMBO J*. 12:2321–2327.
20. Perlot, T., F.W. Alt, C.H. Bassing, H. Suh, and E. Pinaud. 2005. Elucidation of IgH intronic enhancer functions via germ-line deletion. *Proc. Natl. Acad. Sci. USA*. 102:14362–14367.
21. Xu, Y., L. Davidson, F.W. Alt, and D. Baltimore. 1996. Deletion of the Ig kappa light chain intronic enhancer/matrix attachment region impairs but does not abolish V kappa J kappa rearrangement. *Immunity*. 4:377–385.
22. Gorman, J.R., N. van der Stoep, R. Monroe, M. Cogne, L. Davidson, and F.W. Alt. 1996. The Ig kappa 3′ enhancer influences the ratio of Ig kappa versus Ig lambda B lymphocytes. *Immunity* 5:241–252.
23. Inlay, M., F.W. Alt, D. Baltimore, and Y. Xu. 2002. Essential roles of the kappa light chain intronic enhancer and 3′ enhancer in kappa rearrangement and demethylation. *Nat. Immunol*. 3:463–468.
24. Perry, R.P., D.E. Kelley, C. Coleclough, J.G. Seidman, P. Leder, S. Tonegawa, G. Matthyssens, and M. Weigert. 1980. Transcription of mouse kappa chain genes: implications for allelic exclusion. *Proc. Natl. Acad. Sci. USA*. 77:1937–1941.
25. Van Ness, B.G., M. Weigert, C. Coleclough, E.L. Mather, D.E. Kelley, and R.P. Perry. 1981. Transcription of the unrearranged mouse C kappa locus: sequence of the initiation region and comparison of activity with a rearranged V kappa-C kappa gene. *Cell*. 27:593–602.
26. Schlissel, M.S., and D. Baltimore. 1989. Activation of immunoglobulin kappa gene rearrangement correlates with induction of germline kappa gene-transcription. *Cell*. 58:1001–1007.
27. Liang, H.E., L.Y. Hsu, D. Cado, and M.S. Schlissel. 2004. Variegated transcriptional activation of the immunoglobulin kappa locus in pre-b cells contributes to the allelic exclusion of light-chain expression. *Cell*. 118:19–29.
28. Ferradini, L., H. Gu, A. De Smet, K. Rajewsky, C.A. Reynaud, and J.C. Weill. 1996. Rearrangement-enhancing element upstream of the mouse immunoglobulin kappa chain J cluster. *Science*. 271:1416–1420.
29. Cocea, L., A. De Smet, M. Saghatchian, S. Fillatreau, L. Ferradini, S. Schurmans, J.C. Weill, and C.A. Reynaud. 1999. A targeted deletion of a region upstream from the Jκ cluster impairs κ chain rearrangement in cis in mice and in the 103/bcl2 cell line. *J. Exp. Med*. 189:1443–1450.
30. Casellas, R., M. Jankovic, G. Meyer, A. Gazumyan, Y. Luo, R. Roeder, and M. Nussenzweig. 2002. OcaB is required for normal transcription and V(D)J recombination of a subset of immunoglobulin kappa genes. *Cell*. 110:575–585.
31. Inlay, M., and Y. Xu. 2003. Epigenetic regulation of antigen receptor rearrangement. *Clin. Immunol*. 109:29–36.
32. Mostoslavsky, R., N. Singh, A. Kirillov, R. Pelanda, H. Cedar, A. Chess, and Y. Bergman. 1998. Kappa chain monoallelic demethylation and the establishment of allelic exclusion. *Genes Dev*. 12:1801–1811.
33. Cherry, S.R., C. Beard, R. Jaenisch, and D. Baltimore. 2000. V(D)J recombination is not activated by demethylation of the kappa locus. *Proc. Natl. Acad. Sci. USA*. 97:8467–8472.
34. Chowdhury, D., and R. Sen. 2001. Stepwise activation of the immunoglobulin mu heavy chain gene locus. *EMBO J*. 20:6394–6403.
35. Chowdhury, D., and R. Sen. 2003. Transient IL-7/IL-7R signaling provides a mechanism for feedback inhibition of immunoglobulin heavy chain gene rearrangements. *Immunity*. 18:229–241.
36. Maes, J., L.P. O'Neill, P. Cavelier, B.M. Turner, F. Rougeon, and M. Goodhardt. 2001. Chromatin remodeling at the Ig loci prior to V(D)J recombination. *J. Immunol*. 167:866–874.
37. Goldmit, M., Y. Ji, J. Skok, E. Roldan, S. Jung, H. Cedar, and Y. Bergman. 2005. Epigenetic ontogeny of the Igk locus during B cell development. *Nat. Immunol*. 6:198–203.
38. McMurry, M.T., and M.S. Krangel. 2000. A role for histone acetylation in the developmental regulation of VDJ recombination. *Science*. 287:495–498.
39. Romanow, W.J., A.W. Langerak, P. Goebel, I.L. Wolvers-Tettero, J.J. van Dongen, A.J. Feeney, and C. Murre. 2000. E2A and EBF act in synergy with the V(D)J recombinase to generate a diverse immunoglobulin repertoire in nonlymphoid cells. *Mol. Cell*. 5:343–353.
40. Inlay, M.A., H. Tian, T. Lin, and Y. Xu. 2004. Important roles for E protein binding sites within the immunoglobulin κ chain intronic enhancer in activating Vκ Jκ rearrangement. *J. Exp. Med*. 200:1205–1211.
41. Goebel, P., N. Janney, J.R. Valenzuela, W.J. Romanow, C. Murre, and A.J. Feeney. 2001. Localized gene-specific induction of accessibility to V(D)J recombination induced by E2A and early B cell factor in nonlymphoid cells. *J. Exp. Med*. 194:645–656.

42. Eckner, R., T.P. Yao, E. Oldread, and D.M. Livingston. 1996. Interaction and functional collaboration of p300/CBP and bHLH proteins in muscle and B-cell differentiation. *Genes Dev.* 10:2478–2490.
43. Qiu, Y., A. Sharma, and R. Stein. 1998. p300 mediates transcriptional stimulation by the basic helix-loop-helix activators of the insulin gene. *Mol. Cell. Biol.* 18:2957–2964.
44. Massari, M.E., P.A. Grant, M.G. Pray-Grant, S.L. Berger, J.L. Workman, and C. Murre. 1999. A conserved motif present in a class of helix-loop-helix proteins activates transcription by direct recruitment of the SAGA complex. *Mol. Cell.* 4:63–73.
45. Ehlich, A., S. Schaal, H. Gu, D. Kitamura, W. Muller, and K. Rajewsky. 1993. Immunoglobulin heavy and light chain genes rearrange independently at early stages of B cell development. *Cell.* 72:695–704.
46. Novobrantseva, T.I., V.M. Martin, R. Pelanda, W. Muller, K. Rajewsky, and A. Ehlich. 1999. Rearrangement and expression of immunoglobulin light chain genes can precede heavy chain expression during normal B cell development in mice. *J. Exp. Med.* 189:75–88.
47. Gilfillan, S., A. Dierich, M. Lemeur, C. Benoist, and D. Mathis. 1993. Mice lacking TdT: mature animals with an immature lymphocyte repertoire. *Science.* 261:1175–1178.
48. Komori, T., A. Okada, V. Stewart, and F.W. Alt. 1993. Lack of N regions in antigen receptor variable region genes of TdT-deficient lymphocytes. *Science.* 261:1171–1175.
49. Curry, J.D., L. Li, and M.S. Schlissel. 2005. Quantification of Jkappa signal end breaks in developing B cells by blunt-end linker ligation and qPCR. *J. Immunol. Methods.* 296:19–30.
50. Casellas, R., T.A. Shih, M. Kleinewietfeld, J. Rakonjac, D. Nemazee, K. Rajewsky, and M.C. Nussenzweig. 2001. Contribution of receptor editing to the antibody repertoire. *Science.* 291:1541–1544.
51. Novobrantseva, T., S. Xu, J.E. Tan, M. Maruyama, S. Schwers, R. Pelanda, and K.P. Lam. 2005. Stochastic pairing of Ig heavy and light chains frequently generates B cell antigen receptors that are subject to editing in vivo. *Int. Immunol.* 17:343–350.
52. Verkoczy, L.K., A.S. Martensson, and D. Nemazee. 2004. The scope of receptor editing and its association with autoimmunity. *Curr. Opin. Immunol.* 16:808–814.
53. Gay, D., T. Saunders, S. Camper, and M. Weigert. 1993. Receptor editing: an approach by autoreactive B cells to escape tolerance. *J. Exp. Med.* 177:999–1008.
54. Nussenzweig, M.C. 1998. Immune receptor editing: revise and select. *Cell.* 95:875–878.
55. Nemazee, D., and M. Weigert. 2000. Revising B cell receptors. *J. Exp. Med.* 191:1813–1817.
56. Retter, M.W., and D. Nemazee. 1998. Receptor editing occurs frequently during normal B cell development. *J. Exp. Med.* 188:1231–1238.
57. Bergman, Y., A. Fisher, and H. Cedar. 2003. Epigenetic mechanisms that regulate antigen receptor gene expression. *Curr. Opin. Immunol.* 15:176–181.
58. Goldmit, M., M. Schlissel, H. Cedar, and Y. Bergman. 2002. Differential accessibility at the {kappa} chain locus plays a role in allelic exclusion. *EMBO J.* 21:5255–5261.
59. Frommer, M., L.E. McDonald, D.S. Millar, C.M. Collis, F. Watt, G.W. Grigg, P.L. Molloy, and C.L. Paul. 1992. A genomic sequencing protocol that yields a positive display of 5-methylcytosine residues in individual DNA strands. *Proc. Natl. Acad. Sci. USA.* 89:1827–1831.
60. Nikolajczyk, B.S., J.A. Sanchez, and R. Sen. 1999. ETS protein-dependent accessibility changes at the immunoglobulin mu heavy chain enhancer. *Immunity.* 11:11–20.
61. Ernst, P., and S.T. Smale. 1995. Combinatorial regulation of transcription II: the immunoglobulin mu heavy chain gene. *Immunity.* 2:427–438.
62. Cockerill, P.N., and W.T. Garrard. 1986. Chromosomal loop anchorage of the kappa immunoglobulin gene occurs next to the enhancer in a region containing topoisomerase II sites. *Cell.* 44:273–282.
63. Cockerill, P.N., M.H. Yuen, and W.T. Garrard. 1987. The enhancer of the immunoglobulin heavy chain locus is flanked by presumptive chromosomal loop anchorage elements. *J. Biol. Chem.* 262:5394–5397.
64. Jenuwein, T., W.C. Forrester, L.A. Fernandez-Herrero, G. Laible, M. Dull, and R. Grosschedl. 1997. Extension of chromatin accessibility by nuclear matrix attachment regions. *Nature.* 385:269–272.
65. Scheuermann, R.H., and W.T. Garrard. 1999. MARs of antigen receptor and co-receptor genes. *Crit. Rev. Eukaryot. Gene Expr.* 9:295–310.
66. Sakai, E., A. Bottaro, L. Davidson, B.P. Sleckman, and F.W. Alt. 1999. Recombination and transcription of the endogenous Ig heavy chain locus is effected by the Ig heavy chain intronic enhancer core region in the absence of the matrix attachment regions. *Proc. Natl. Acad. Sci. USA.* 96:1526–1531.
67. Yi, M., P. Wu, K.W. Trevorrow, L. Claflin, and W.T. Garrard. 1999. Evidence that the Igkappa gene MAR regulates the probability of premature V-J joining and somatic hypermutation. *J. Immunol.* 162:6029–6039.
68. Hale, M.A., and W.T. Garrard. 1998. A targeted kappa immunoglobulin gene containing a deletion of the nuclear matrix association region exhibits spontaneous hyper-recombination in pre-B cells. *Mol. Immunol.* 35:609–620.
69. Scheuermann, R.H., and U. Chen. 1989. A developmental-specific factor binds to suppressor sites flanking the immunoglobulin heavy-chain enhancer. *Genes Dev.* 3:1255–1266.
70. Kosak, S.T., J.A. Skok, K.L. Medina, R. Riblet, M.M. Le Beau, A.G. Fisher, and H. Singh. 2002. Subnuclear compartmentalization of immunoglobulin loci during lymphocyte development. *Science.* 296:158–162.
71. Fuxa, M., J. Skok, A. Souabni, G. Salvagiotto, E. Roldan, and M. Busslinger. 2004. Pax5 induces V-to-DJ rearrangements and locus contraction of the immunoglobulin heavy-chain gene. *Genes Dev.* 18:411–422.
72. Roldan, E., M. Fuxa, W. Chong, D. Martinez, M. Novatchkova, M. Busslinger, and J.A. Skok. 2005. Locus 'decontraction' and centromeric recruitment contribute to allelic exclusion of the immunoglobulin heavy-chain gene. *Nat. Immunol.* 6:31–41.
73. Sayegh, C., S. Jhunjhunwala, R. Riblet, and C. Murre. 2005. Visualization of looping involving the immunoglobulin heavy-chain locus in developing B cells. *Genes Dev.* 19:322–327.
74. Liu, Z., and W.T. Garrard. 2005. Long-range interactions between three transcriptional enhancers, active Vkappa gene promoters, and a 3′ boundary sequence spanning 46 kilobases. *Mol. Cell. Biol.* 25:3220–3231.
75. Gu, H., J.D. Marth, P.C. Orban, H. Mossmann, and K. Rajewsky. 1994. Deletion of a DNA polymerase beta gene segment in T cells using cell type-specific gene targeting. *Science.* 265:103–106.
76. Kim, J.S., and C. Jobin. 2005. The flavonoid luteolin prevents lipopolysaccharide-induced NF-kappaB signalling and gene expression by blocking IkappaB kinase activity in intestinal epithelial cells and bone-marrow derived dendritic cells. *Immunology.* 115:375–387.